Magnetic and electronic properties of the ferroelectric-photovoltaic ordered double perovskite $CaMnTi_2O_6$ investigated by x-ray absorption spectroscopies

Javier Herrero-Martín,[1,*] Javier Ruiz-Fuertes,[2,3] Thomas Bernert,[4] Monika Koch-Müller,[5] Eiken Haussühl,[6] and José Luis García-Muñoz[7]

[1]*ALBA Synchrotron Light Facility, 08290 Cerdanyola del Vallès, Barcelona, Spain*
[2]*DCITIMAC, MALTA Consolider Team, Universidad de Cantabria, 39005 Santander, Spain*
[3]*Departament de Física Aplicada-ICMUV, MALTA Consolider Team, 46100 Burjassot, Spain*
[4]*Max-Planck-Institut für Kohlenforschung, Kaiser-Wilhelm-Platz 1, 45470 Mülheim an der Ruhr, Germany*
[5]*GFZ Potsdam, Sektion 4.3, Telegrafenberg, 14473 Potsdam, Germany*
[6]*Institut für Geowissenschaften, Goethe-Universität, Altenhöferallee 1, 60438 Frankfurt am Main, Germany*
[7]*Institut de Ciència de Materials de Barcelona, ICMAB-CSIC, Campus Universitari de Bellaterra, 08193 Bellaterra, Spain*

(Received 5 March 2018; revised manuscript received 15 May 2018; published 15 June 2018)

The ferroelectric and magnetic phases of the double perovskite $CaMnTi_2O_6$ with A-site order have been investigated by soft x-ray absorption and magnetic circular dichroism. All spectra point to a very ionic state of divalent Mn and tetravalent Ti atoms. The effects of the crystal field produced by O ligands around tetravalent titanium and the dissimilar Mn1 and Mn2 sites were investigated. Both the so-called square-planar and the octahedrally coordinated Mn sites spectroscopically contribute in a rather similar way, with little influence by the oxygen environment. Multiplet calculations suggest a small $O\,2p$-Ti $3d$ charge-transfer component in the FE phase. Magnetic symmetry calculations were performed to determine probable configurations of Mn spins compatible with the acentric $P4_2mc$ structure and, in combination with the computational magnetic results in Inorg. Chem. **56**, 11854 (2017), we have identified the $P4'_2m'c$ as the most likely magnetic space group keeping invariant the unit cell below T_N. This symmetry forces the sign of the magnetic coupling along the Mn columns parallel to c to reverse with respect to the coupling between neighboring columns. Below T_N, the dichroic magnetization loops at the Mn L_3 edge confirm the absence of spontaneous ferromagnetism, although a very small field-induced spin polarization was detected in the sample.

DOI: 10.1103/PhysRevB.97.235129

I. INTRODUCTION

Perovskite oxides have been investigated tirelessly during the last decades as a source of a plethora of physical phenomena such as charge ordering, colossal magnetoresistance, superconductivity, ferroelectricity, colossal magnetoelectric effects, or photovoltaic response [1–4]. So far, room-temperature ferroelectric (FE) materials are generally associated to single perovskites based on second-order Jahn–Teller (SOJT) active cations with d^0(Ti^{4+}, Zr^{4+}, Nb^{5+}) or s^2(Pb^{2+}, Bi^{3+}) valence band electron configuration. These SOJT active cations are prone to anisotropic covalent bonding with ligands inducing structural distortions that may eventually lead to the appearance of a collective polar mode and a macroscopic electric dipolar moment $\boldsymbol{P}$, whenever the relevant distortions do not array generating antiparallel effects.

The recent synthesis by Aimi *et al.* [5] of the type-I ferroelectric $CaMnTi_2O_6$ (CMTO), a novel tetragonal double perovskite (DP) with less common A-site order, proves that A-site ordering and SOJT distortions can couple to enable FE. The polar structure of CMTO consists of a tetragonal structure described in the noncentrosymmetric space group $P4_2mc$ in which the octahedral B positions are occupied by Ti^{4+} ions. In the A-site, Ca^{2+} alternate with Mn^{2+} ions along a and b axes forming a columnar ordered structure described in Fig. 1(a). In addition, the two Mn positions exhibit different coordination: tetrahedral at Mn1 sites and pseudosquare planar at Mn2 [Fig. 1(a)]. In contrast to the centrosymmetric DP structure adopted by $CaFeTi_2O_6$($P4_2/nmc$) [6], Ti^{4+} ions in $CaMnTi_2O_6$ are shifted from the basal plane of the octahedron along the c axis, losing spatial inversion [5]. For its part, Mn^{2+} ions with square-planar coordination suffer a similar displacement [see the shift of Mn2 atoms along z direction in Fig. 1(a)]. Indeed, the reduced crystal field energy provided by their d^5 valence band configuration allows high coordination symmetry freedom. As a consequence, a remnant polarization of 3.5 mC/cm^2 gets measured at room temperature.

In the novel mechanism known as "hybrid improper ferroelectricity" the condensation of two nonpolar lattice modes (e.g., associated to oxygen octahedral rotations or tilts) can favor the activation of a third mode, the latter of polar nature [7–9]. Gou *et al.* [10] have shown that this mechanism can give account of the polar distortion and FE in CMTO. The parent phase of the polar CMTO structure is the $P4/mmm$ space group ($a^0a^0c^0$, distortion free, in Glazer notation [11]). The ground distorted FE $P4_2mc$ phase is a nonmaximal subgroup of the parent phase, and it results from the activation of three primary modes (A_4^+, Z_2^-, and Γ_3^-). The two former—of larger amplitude—correspond to in-phase $a^+a^+c^0$ and

*jherrero@cells.es

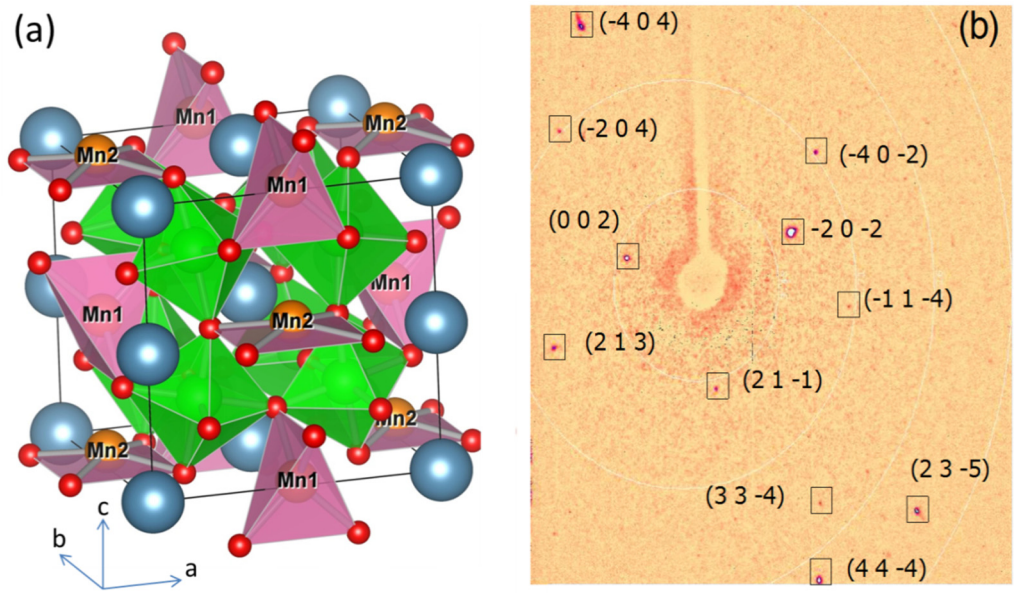

FIG. 1. (a) Crystallographic projection of the polar phase of $CaMnTi_2O_6$ (space group $P4_2mc$). The two positions of Ca atoms are represented in grey; TiO_6 octahedra appear in green color; the two independent Mn sites are easily identifiable: Mn1 in tetrahedral coordination (purple) and Mn2 in square-planar coordination (orange). (b) X-ray diffraction frame of one of the single crystals ($30 \times 20 \times 10\,\mu$m) that formed the sample used in our experiments.

out-of-phase $a^0a^0c^-$ TiO_6 rotations, transforming the parent group into the maximal subgroup $P4_2/nmc$ ($a_0^+a_0^+c_0^-$, nonpolar). But the lowest energy is reached by activation of the polar mode represented by the irrep Γ_3^- (irreducible representation permitting polar displacements of Ti and Mn cations), which transforms the $P4_2/nmc$ symmetry into the final FE $P4_2mc$ structure ($a_0^+a_0^+c_0^-$). As mentioned above, these displacements and hence the Γ_3^- mode are favored by the Ti^{4+} electronic configuration.

The FE phase of CMTO persists at ambient pressure up to $T_C = 630$ K [5] or at ambient temperature up to ~7 GPa [6] when a second-order structural phase transition suppresses the distortion associated to the Γ_3^- irrep, and the $P4_2mc$ symmetry gives way to its supergroup $P4_2/nmc$ and the paraelectric (PE) phase. When the system enters the PE phase ($P4_2/nmc$) either by increasing the temperature or hydrostatic pressure the off-center atomic displacement of Ti completely vanishes, while the shift of Mn2 cations from the center of the square-plane gets reduced to half its original size with 50% of the Mn2 ions being shifted up and the other 50% down. First-principles calculations point to the appearance of a nonzero macroscopic spontaneous polarization $\boldsymbol{P}$ by cooperative atomic displacements involving Mn and Ti. In addition, a moderate piezoelectric response would be at play under external stress or strain applied along the polar axis, as well as interesting photovoltaic capabilities, mostly dependent on planar Mn-O bonds [10].

Concerning the magnetic behavior of CMTO, it shows a Weiss temperature of ~ -32 K and undergoes a λ-type phase transition at Néel temperature $T_N = 10$ K into an antiferromagnetic (AFM) structure that coexists with the FE order [5]. The actual magnetic order in the system remains unknown and the magnetoelectric coupling is expected to be small [10].

In view of all these considerations, $CaMnTi_2O_6$ would form part of the new class of perovskites known as Mott multiferroics, based on two metals: one with empty d orbitals shell and the other with the same band half-filled, showing room-temperature FE, antiferromagnetic order, and a reduced band gap that could be exploited for the conversion of light into energy [12]. To this extent, CMTO is most likely the first compound of this class where one metal lies at A and the other at the B perovskite generic site.

In this work, we aim at describing the $3d$ band electronic configuration of Mn and Ti cations in $CaMnTi_2O_6$ and investigating its low-temperature magnetic properties. We first discuss our soft x-ray absorption and circular magnetic dichroism experimental results at Mn and Ti $L_{2,3}$ edges, followed by charge transfer multiplet calculations. Then, we present a magnetic symmetry group analysis of the most likely spins arrangement below Néel temperature. The technical difficulties found to prepare large amounts of CMTO explain the absence of any neutron data. We have applied the general principle of maximal symmetry, in combination with the results of some earlier reports, to identify the most favorable magnetic space group (MSG) compatible with the polar $P4_2mc$ crystalline structure of CMTO.

II. EXPERIMENTAL DETAILS

$CaMnTi_2O_6$ was synthesized using pure ilmenite-type $MnTiO_3$ and $CaTiO_3$ sealed inside a platinum capsule at 7 GPa and 1700 °C in a multianvil press for 30 min following the work by Aimi *et al.* [5]. The multianvil experiment was performed at GFZ Potsdam with an 18/11 assembly, which was calibrated at room temperature against the phase transitions in Bi metal [13,14]. Calibrations at high temperature are based on the following phase transitions: garnet-perovskite for $CaGeO_3$

[15] and coesite-stishovite for SiO_2 [16]. Stepped graphite heaters were employed, and temperatures were measured with type-C thermocouples. We obtained orange single crystals 10–50 μm in size embedded in powder. Pure phase crystals of $CaMnTi_2O_6$ were obtained as confirmed by single-crystal x-ray diffraction (XRD) experiments employing an XCalibur four-circle diffractometer (Rigaku-Oxford diffraction) with Mo-K_α radiation and a CCD detector (Sapphire 3) placed at 42 mm from the sample. Synchrotron powder XRD experiments ($\lambda = 0.29036$ Å) were also carried out as a function of pressure at the Extreme Conditions P2.2 beamline at PETRA III (Germany). High-pressure characterization by means of second-harmonic generation (SHG), Raman spectroscopy and single-crystal XRD (SXRD) experiments were carried out using Boehler-Almax diamond-anvil cells (DACs) [6].

Soft x-ray absorption spectroscopy (XAS) and x-ray magnetic circular dichroism (XMCD) measurements at the Mn and Ti $L_{2,3}$ edges were performed in the HECTOR cryomagnet endstation at the BL29-BOREAS beamline of the ALBA Synchrotron in Barcelona, Spain [17]. Micrometric single crystals of $CaMnTi_2O_6$ were deposed and pressed onto a piece of metallic In film sticked to a Cu sample holder to optimize thermal and electrical conductivity since all data were recorded in a total electron yield (TEY) mode. The pressure of the cryomagnet was kept at 1×10^{-10} mbar during measurements. The XMCD spectra were recorded using alternatively left and right circularly polarized x rays produced by an APPLE II undulator and a superconducting split coil setup generating a magnetic field up to 6 T in the direction of propagation of the incident photons. The total incoming radiation flux was about 5×10^{11} photons/s with an energy resolution of ~50 meV. Charge-transfer multiplet calculations were performed with CTM4XAS [18] to simulate and help interpreting the experimentally measured XAS and XMCD spectra. Crystallographic tools from the Bilbao Crystallographic server [19–21] and the ISOTROPY software suite [22] were also used.

III. RESULTS AND DISCUSSION

One of the measured SXRD frames using the XCalibur four-circle diffractometer is shown in Fig. 1(b). All the observed reflections at ambient temperature were successfully indexed to the polar phase of $CaMnTi_2O_6$ (space group $P4_2mc$). The raw data were processed (indexation) and reduced (intensity data reduction) using the CRYSALIS^{PRO} software [23], and finally the structure was solved and refined with SHELX97-2 [24]. Additional details on the SXRD data collection and agreement factors are given in Table I. The refined atomic coordinates, temperature factors and lattice parameters are shown in Table II. Using these numbers, a schematic projection of the CMTO crystal structure is depicted in Fig. 1(a). The refined structure agrees with the description provided in Ref. [5]. In the polar space group $P4_2mc$, this distorted double perovskite has two Ca^{2+} sites, two Mn^{2+} sites, one Ti^{4+} site, and five O^{2-} sites: Ca1 and Ca2 occupy the Wyckoff positions $2a(0, 0, 0)$ and $2b(1/2, 1/2, z)$, respectively; Mn1 and Mn2 lie both at $2b(1/2, 1/2, z)$ sites, with $z(\mathrm{Mn1}) = 0.5162(8)$ and $z(\mathrm{Mn2}) = 0.0557(9)$; Ti and O5 atoms are at $8f$ general positions; finally, O1, O4 are located at $4e$ and O2, O3 at $4d$ positions, respectively.

TABLE I. Single-crystal x-ray diffraction experiment: details of the data collection and agreement factors.

Wavelength (Å)	0.71073
Index ranges	$-9 \leqslant h \leqslant 10$
	$-10 \leqslant k \leqslant 9$
	$-10 \leqslant l \leqslant 10$
Measured reflections	6721
Unique reflections	648
Reflect. $F > 4\sigma(F)$	492
Parameters	43
R_{int}	0.055
R_σ	0.0318
R_1	0.0664
wR_2	0.1324
S (Goodness of fit)	1.167

A. X-ray absorption and magnetic circular dichroism at Mn and Ti $L_{2,3}$ edges

All Mn atoms in $CaMnTi_2O_6$ are expected to lie in a divalent oxidation state. This is supported by the measured XAS spectrum shown in Fig. 2, which is characteristic of Mn^{2+} in a high-spin configuration (d^5 up, d^0 down spins), with little variations depending on the local symmetry around Mn ions. Indeed, the magnetic $^6A_2$ ground state gets little affected by the coordination environment due to the large ionicity of Mn^{2+} [25,26]. This will get further commented later when discussing multiplet calculations. As in the case of XAS, the XMCD spectrum (also plotted in Fig. 2) does contain the spectroscopic contribution from Mn1 (T_d) and Mn2 (C_{4h}) Mn sites. The sizeable XMCD signal at 5 K is likely to find its roots in a large magnetic susceptibility at low temperatures rather than in a ferromagnetic component. Interestingly, the integral of the magnetic dichroic signal (directly related to the sign and

TABLE II. Main structural parameters, atomic coordinates, and temperature factors U_{eq} and U_{iso} expressed in Å^2 for $CaMnTi_2O_6$ obtained by single-crystal x-ray diffraction at 300 K. For Ca, Mn, and Ti atoms, the refinement was done anisotropically and therefore their U_{eq} are shown whereas for the O atoms the refinement was done isotropically and the U_{iso} are presented. Lattice parameters are in angstroms and the volume V in Å^3.

$P4_2mc$		$T = 300$ K			
Atoms	WP	x	y	z	$U_{\mathrm{eq}}/U_{\mathrm{iso}}$
Ca1	$2a$	0	0	0	0.0150(16)
Ca2	$2b$	1/2	1/2	0.0385(9)	0.030(3)
Mn1	$2c$	0	1/2	0.5162(8)	0.0268(13)
Mn2	$2c$	0	1/2	0.0557(9)	0.037(3)
Ti	$8f$	0.2550(4)	0.2461(4)	0.270(11)	0.0165(5)
O1	$4e$	0.291(2)	1/2	0.289(3)	0.031(4)
O2	$4d$	0.294(2)	0	0.820(3)	0.031(4)
O3	$4d$	0.202(2)	0	0.227(2)	0.021(3)
O4	$4e$	0.210(2)	1/2	0.717(3)	0.025(4)
O5	$8f$	0.1976(14)	0.2805(14)	0.013(2)	0.023(2)
$a = 7.5376(2)$ $b = 7.5376(2)$ $c = 7.6002(4)$					
$V = 431.81(3)$ Å, $Z = 4$					

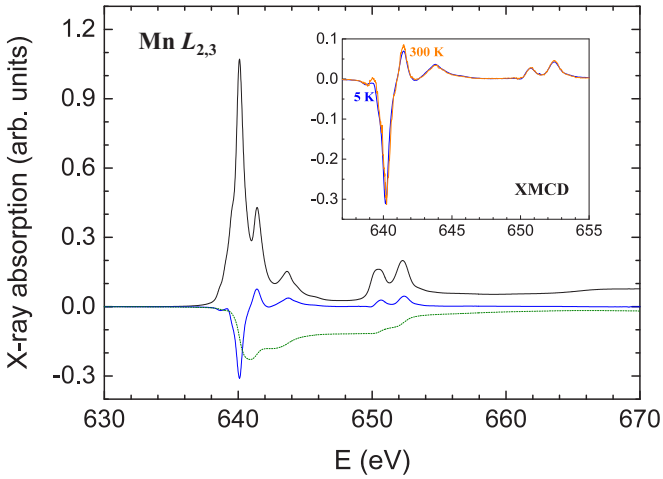

FIG. 2. Experimental x-ray absorption (solid, black line) and x-ray magnetic circular dichroism (solid, blue) spectra of $CaMnTi_2O_6$ across the Mn $L_{2,3}$ edges at 5 K and 6 T applied field. The dashed, green line corresponds to the XMCD integration curve used for spin and orbital sum rules. (Inset) Comparison of the XMCD spectra at 5 K (blue) and 300 K (orange). The latter has been normalized to the low-T spectrum applying the multiplicative factor 11.7.

magnitude of the orbital angular part of the atomic magnetic moment) does not fully converge to zero beyond the Mn L_2 edge. This indicates that, in contrast to the ideally ionic case, a small orbital magnetic moment is at play. Quantitatively, the spin and orbital sum rules [27,28] yield a spin moment value $m_S = 0.733(9)$ and orbital moment $m_L = 0.026(1)$ at 5 K (i.e., in the AFM phase), and so $m_L/m_S = 0.035(3)$. This confirms that, as expected for this Mn^{2+}-based system, the long-range magnetic order at such a low temperature is mainly due to the weakness of spin-spin exchange interactions [10]. The evolution of both the XMCD (Fig. 2, inset) and XAS (not shown) spectra as a function of temperature does not exhibit major variations in the 5 to 300 K range. However, a deeper inspection reveals some differences, since at 25 K (above T_N) we measure $m_S = 0.558(2)$ and $m_L = 0.003(7)$, i.e., the orbital contribution is negligible above T_N.

A disclosure of the individual x-ray spectroscopic contribution of each of the two Mn sites requires a theoretical analysis. For this reason, the multiplet formalism was employed to simulate the XAS and XMCD across both Ti and Mn $L_{2,3}$ edges. In particular, the x-ray absorption cross section of Mn^{2+} ions is mostly determined by multipole electron-electron Coulomb interactions. Also, divalent manganese is characterized by large charge-transfer energy values (due to high ionicity) and limited crystal field energies. Figure 3 contains selected calculations for XAS and XMCD spectra of CMTO using different local symmetries and electronic parameters for Mn $3d$ states (see Fig. 3, top panel, and details in Ref. [29]). The best XAS spectrum for Mn1 sites is obtained using T_d symmetry and a crystal field value ($10Dq$) around 0.5 eV, the charge transfer to oxygen being neglected. For Mn2 sites, we tried different energy level schemes for d orbitals. As compared to the cubic case, a square-planar local symmetry around the photoabsorbing transition-metal is characterized by a breaking of e_g states degeneracy; a large

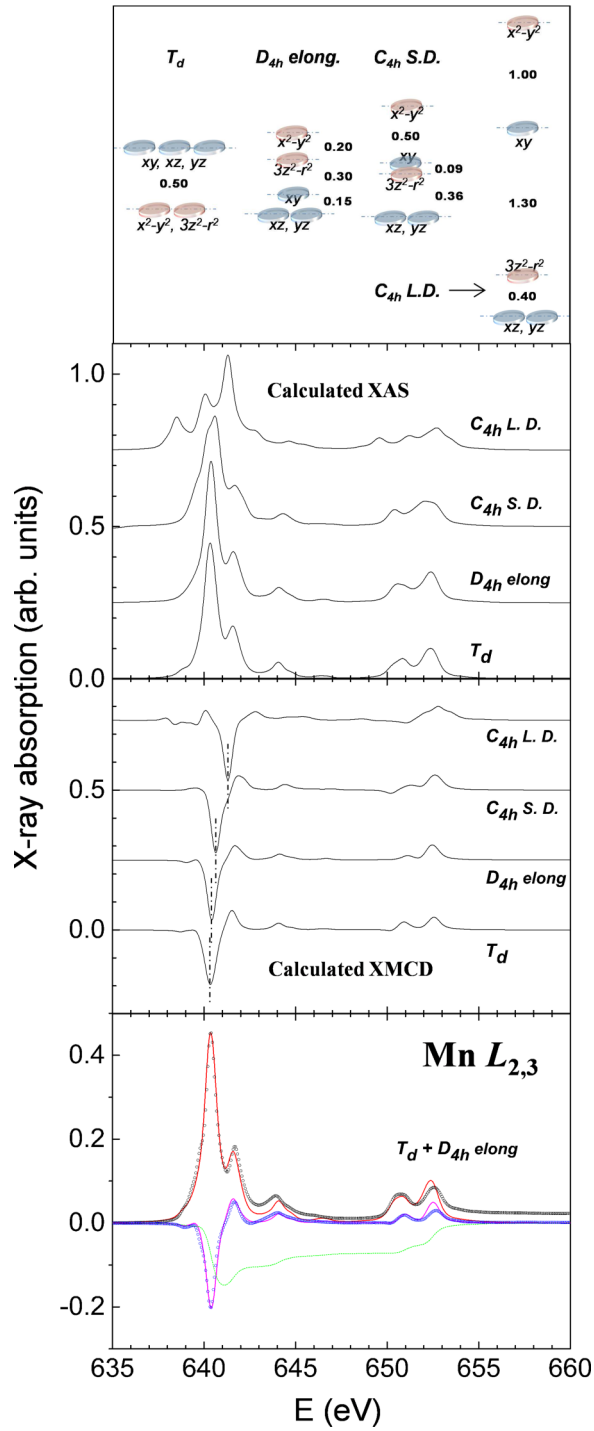

FIG. 3. Multiplet spectra calculated for Mn atoms in $CaMnTi_2O_6$ across $L_{2,3}$ absorption edges. Panels from top to bottom respectively show (i) a scheme of atomic $3d$ orbital relative energies (eV) for each local symmetry around Mn atoms, (ii) XAS, and (iii) XMCD spectra for these local structures, as commented in the main text, and (iv) the best XAS (red) and XMCD (magenta) simulated spectra for $CaMnTi_2O_6$ after considering the relative weight of tetrahedral and pseudo square-planar Mn^{2+} sites. The green dashed curve corresponds to the corresponding XMCD simulated integral curve. The experimental data (open circles) shown in Fig. 2 are also plotted for comparison. Note that nonresonant absorption has not been subtracted from the experimental data, and that it is not comprehended in calculated spectra.

decrease in the d_{z2} orbital energy (E_{z2}) is realized such that $E_{dz2} < E_{dxy}$ holds. We illustrate the spectroscopic effects of this hypothesis by means of C_{4h} SD and C_{4h} LD curves, where SD and LD stand for small and large distortion, respectively, and refer to the magnitude of $10Dq$ used: 0.5 for SD and 1.0 eV for LD. This also applies to XMCD calculations, where, in order to account for the effect produced by an external applied magnetic field over the studied sample, a molecular field of 0.01 eV was incorporated. If we consider that both the experimental XAS and XMCD spectra of CMTO are very similar to the calculated ones just for T_d symmetry, one can guess that Mn2 sites cannot yield markedly different spectroscopic results. This leads us to dismiss the C_{4h} LD calculation. Figure 3 also shows the spectra obtained for a nominally tetragonal calculation ($E_{dx2-y2} > E_{dz2}$ and $E_{dz2} > E_{dxy}$) tagged as "D_{4h} elong" where the apical Mn-O bondlengths are well beyond the basal ones. The parameter values here chosen make d orbital energies not to be far from those in C_{4h} SD calculation. However, in D_{4h} elong, the apical distortion is not as large as to produce the reversal of d_{z2} and d_{xy} levels [29]. It turns that "D_{4h} elong" yields the best results when (i) inspecting both the average XAS and XMCD curves it provides after combination with the aforementioned T_d calculation spectra—we name this simulation "$T_d + D_{4h}$ elong."—(Fig. 3, bottom panel) and (ii) comparing these simulations to the actually recorded spectra. Despite not shown, we can indicate that the "$T_d + C_{4h}$ SD" simulation is particularly poorer than "$T_d + D_{4h}$ elong." at the Mn L_2 edge and fails at reproducing the correct relative energy position of the experimental main spectral features at the Mn L_3 edge (at 640 eV) of the XAS and XMCD spectra.

We can draw several conclusions from our calculations. Firstly, the XAS and XMCD signature of both Mn1 and Mn2 sites is very similar. As earlier commented, this is not a surprise for divalent manganese. For this reason, it becomes difficult to specifically ascribe the measured XMCD signal to any of the two Mn sites. Related to this, the small differences observed between the 300-K and 5-K spectra (Fig. 2, inset) do not allow a clear correlation to variations in the spectral weighing of the best calculations performed for the Mn1 and Mn2 sites. Finally, our calculations point to an orbital scheme that would better suit a highly distorted tetragonal local structure around Mn2 sites than a proper square-planar symmetry. Further geometrical details about the Mn2 sites can be found in Table S2 of Ref. [5]. At 300 K, the pseudosquare-planar coordination is severely distorted and the four Mn2-O5 bonds present 2.190(4) Å. The bondlength associated to the pair of apical oxygens is 2.456(4) Å [5].

After having discussed the large influence that the characteristic ionicity of divalent Mn ions has on their x-ray spectroscopic fingerprint, we turn our look at the Ti $L_{2,3}$ absorption edges. The experimental XAS and XMCD spectra recorded at 5 K are plotted in Fig. 4(a). As expected, the XAS spectrum reminds of that of Ti in the tetravalent state (atomic ground state $^1S_0$) seen in other compounds [30–32]. Contrarily to the Mn^{2+} case, the XAS spectrum here is fairly proportional to the density of free states (DOS) allowed by the $2p \rightarrow 3d$ dipolar transition just above the Fermi level due to almost complete absence of intraband electron-electron interactions. Thanks to this, the main spectral features can be confidently assigned to t_{2g} and e_g states in each of the two absorption edges. Thus one can extract an approximate value for the crystal field energy

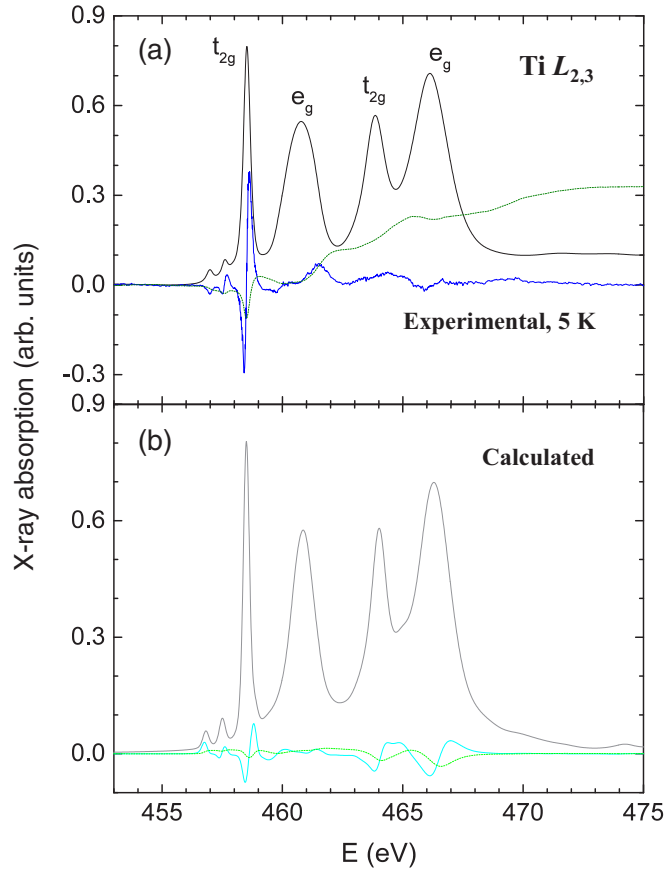

FIG. 4. (a) Experimental x-ray absorption (solid, black line) and x-ray magnetic circular dichroism (solid, blue) spectra of $CaMnTi_2O_6$ across the Ti $L_{2,3}$ edges at 5 K and 6 T applied field. The latter signal has been multiplied by a factor 30 for convenience. The dashed, green line corresponds to the XMCD integral used for spin and orbital sum rule calculations. The correspondence of the different spectroscopic features to t_{2g}- and e_g-symmetry empty $3d$ states is indicated; (b) Ti $L_{2,3}$ calculated XAS (solid, grey line), XMCD (solid, light blue; multiplied by 30), and XMCD integral (dashed, green) curves for CMTO.

that may be of later use for CTM (charge transfer multiplet) calculations [33]. In this case, the splitting produced by the O ligands is of 2.2 eV. The smaller structures appearing between 456 and 458 eV are due to spin-forbidden transitions. In spite of the nominally nonmagnetic character of (d^0) Ti^{4+}, and thanks to the great sensitivity of the equipment used at the beamline, a tiny XMCD signal can be recorded under the application of a large enough magnetic field. The shape is typical of a six-coordinated Ti^{4+} cation where the local octahedron gets elongated along the c axis [34]. Concerning quantitative values, we need to remind that Ti shows the smallest energy splitting between L_3 and L_2 absorption edges. This may result in large deviations for the spin sum rule-derived values regardless of the experimental accuracy. In contrast, the calculated orbital moment does not suffer from these limitations because it does only depend on the total integral of the XMCD signal. Keeping in mind the reliability of sum rules commented above about the derived Ti absolute magnetization values, the values found at 5 K and 6 T applied are $m_S = 0.018(3)$ and $m_L = -0.013(2)$, and thus $m_{TOT} = 0.004(3)\,\mu_B$, i.e., nearly zero. The different

sign would reflect an antiparallel alignment of these spin and orbital components as expected by Hund's third rule.

The best calculated XAS and XMCD spectra using the CTM formalism for Ti $L_{2,3}$ edges in CMTO are shown in Fig. 4(b). The ground state is based on the $3d^{\circ}$ configuration, although a $3d^1\underline{L}$ ($\underline{L}$ denotes a ligand hole at neighboring O atoms) excited state is found to weigh up to 1/3 in such a way that the electron occupation would not be strictly zero but 0.33 electrons would in average be present in the d valence band as donated by surrounding O atoms. The agreement of the XAS calculated curve to the experimental spectrum is remarkable. In the case of the XMCD, several features are qualitatively correct, but we see an overestimation in the signal amplitude around the L_2 edge with respect to the L_3 part of the spectrum. This may be due to approximations made in the employed TiO_6 cluster: the degeneracy of $Ti\ 3d\ e_g$ states was broken so as to simulate the effect of the off-center displacement of Ti cations mainly along the c axis, while for t_{2g} states this was left unaffected [29]. Although the integral of the XMCD calculated curve indicates that should there be a nonzero magnetization at the Ti sites, this would keep at a negligible level. We interpret that the small spin and orbital magnetization found at the Ti sites is more likely to originate in a charge transfer from O ligands' $2p$ orbitals rather than in a hypothetical spin polarization of the $2p^5 3d^1$ final state in Ti^{4+} by Mn spins earlier suggested in other titanates [31,32] since the $L_2 : L_3$ amplitude ratio of XMCD features for Ti^{3+} ions (e.g., due to a deficient oxygenation of the CMTO sample) is pretty distinctive [35].

So far, we have considered that the XMCD signal measured at Mn $L_{2,3}$ edges responds to the sizeable magnetic susceptibility at low temperatures without discussing on the actual nature of the magnetic order below $T_N = 10$ K. This will be addressed in the next section. However, first we present an element-specific—in this case Mn—magnetization loop (ML) performed at both sides of the magnetic transition. It was performed by recording the dichroic signal at a fixed energy (at 640 eV, corresponding to the Mn L_3 edge) while sweeping the applied magnetic field, similarly to as a magnetization hysteresis measurement using a conventional magnetometer. After normalization of the XAS signal, XMCD data get scaled with the same factor and the measured magnitude becomes the projected average moment of all Mn atoms. Figure 5 shows the ML recorded at 5 and 25 K in the –6 to +6 T range. At 25 K ($T > T_N$), the ML curves measured are linear, as expected for a paramagnetic (PM) behaviour. At 5 K, the curve measured is not really linear, a small curvature is seen below 2 T indicating a slight field-induced polarization associated to Mn moments that was not observed at 25 K (above T_N). The nonlinear contribution observed within the field interval [−2 T, +2 T] is very small, reproducible, nonhysteretic, and reversible. No magnetic remanence was observed, in agreement with the AFM nature of CMTO. So, this nonlinear component is not related to a spontaneous small FM component but to a reversible very small spin polarization easily induced by the applied magnetic field, and that disappears suppressing the field. Moreover, it appears superimposed to the normal linear susceptibility of an antiferromagnet, clearly visible beyond 2 T: notice that this last contribution is the main one to the total Mn^{2+} spin moment detected at 5 K by XMCD under 6 T. Our XMCD results agree well with the magnetization data

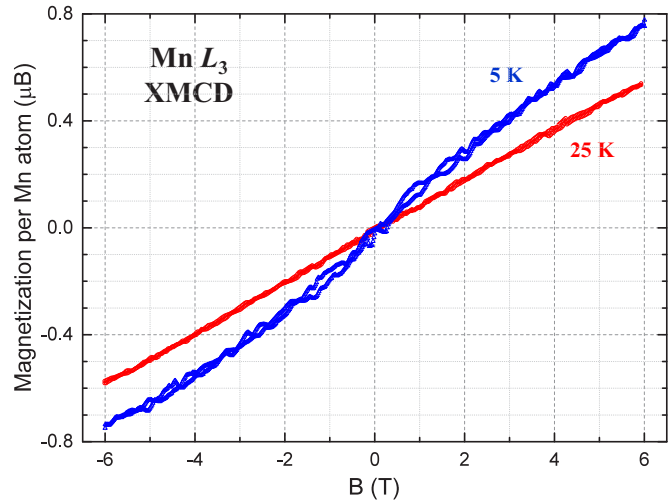

FIG. 5. Magnetization curves for $CaMnTi_2O_6$ as measured at the main feature (at 640 eV) of the Mn $L_{2,3}$ XMCD spectrum at 5 K (blue) and 25 K (red).

reported in the supplementary information of Ref. [5], although the latter only covered the [−1 T, +1 T] applied field range. The univocal identification of the origin of the tiny nonlinear contribution below 2 T demands additional measurements and a larger amount of sample.

B. Magnetic symmetry analysis and spin order

The emergence of AFM order below $T_N \sim 10$ K was reported in Ref. [5] from susceptibility measurements. It is worth noting that the FC/ZFC susceptibility (χ) curves of $CaMnTi_2O_6$ (measured at 10 Oe in Ref. [5]) are undistinguishable above 11 K, but display marked differences below T_N. Only in ZFC conditions, χ(T) shows a clean cusp at the Neel temperature. After the earlier discussion of the magnetic properties by Gou *et al.* [10], based on an estimation of the main magnetic exchange interactions, in this section we perform a symmetry analysis to identify the magnetic symmetry and the magnetic space groups (MSGs) of the more probable low-temperature magnetic structures in CMTO. For that, we make the same assumption as in Ref. [10] that the crystal and magnetic structures have the same unit cell dimensions (null magnetic propagation vector $\boldsymbol{k}$). Several possible magnetic space groups (MSGs) compatible with the polar $P4_2mc$ symmetry and $\boldsymbol{k} = 0$ were considered. As we have confirmed in Sec. III A, only the divalent transition metal (Mn^{2+}) must be considered as magnetic. Therefore we examined the maximal MSGs of the grey group of CMTO $P4_2mc1'$ compatible with ordered Mn moments. They are $P4_2m'c'$ (No. 105.215), $P4_2'm'c$ (No. 105.213), $Cc'c2'$ (No. 37.182), and $Pm'm2'$ (No. 25.59) (in BNS notation [36]). In these MSGs the dimensions of the magnetic unit cell are identical to the PM phase of $CaMnTi_2O_6$ ($\boldsymbol{k} = 0$). The two former groups are already in the standard setting, and the transformation to that setting of the two last is given in Table III. Moreover, notice that there are two independent magnetic sites (Mn1 and Mn2) in the three former MSGs whereas in $Pm'm2'$ these sites split into four independent magnetic Wyckoff sites.

TABLE III. Magnetic space groups compatible with the $P4_2mc$ (No. 105) symmetry of $CaMnTi_2O_6$ and $\boldsymbol{k} = 0$. Maximal subgroups for $\boldsymbol{k} = 0$ assuming the presence of ordered moments only in Mn atoms (no magnetic moments at the Ti positions, in agreement with XMCD results). See explanation in the text.

Magnetic Space Group	***P4$_2$m'c'*** (No. 105.215)	***P4$_2$'m'c*** (No. 105.213)	***Cc'c2'*** (No. 37.182)	***Pm'm2'*** (No. 25.59)
Transformation to standard setting	(**a**, **b**, **c**; 0, 0, 0)	(**a**, **b**, **c**; **0**, 0, 0)	(**a+b**, **-a+b**, **c** ; 0, 0, 0)]	(**-b**, **a**, **c** ; 0, 0, 0)
Magnetic Point Group	**4**m'm' (#13.4.47)	4'm'm (#13.3.46)	m'm2' (#7.3.22)	m'm2' (#7.3.22)
Independent magnetic Wyckoff positions (expressed in parent Tet. setting)	Mn1 (0,1/2,z | 0,0,m$_z$) Mn2 (0,1/2,z | 0,0,m$_z$)	Mn1 (0,1/2,z | 0,0,m$_z$) Mn2 (0,1/2,z | 0,0,m$_z$)	Mn**1** (0,1/2,z | m$_x$,m$_y$,0) Mn**2** (0,1/2,z | m$_x$,m$_y$,0)	Mn11 (0,1/2,z | m$_x$,0,0) Mn12 (1/2,0,z+1/2 | m$_x$,0,0) Mn21 (0,1/2,z | m$_x$,0,0) Mn22 (1/2,0,z+1/2 | m$_x$,0,0)
Magnetic structure	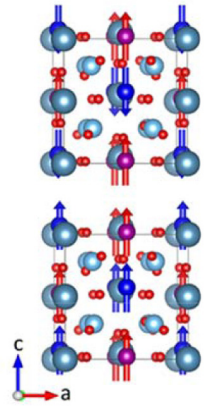	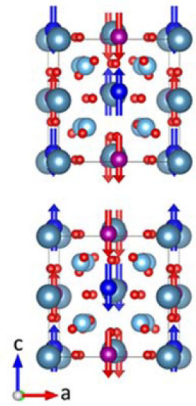	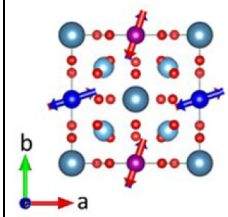	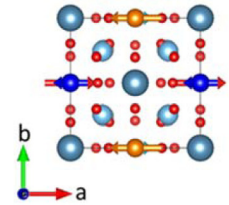

In the $P4_2m'c'$ magnetic symmetry (model_1), the orbit of each independent Mn site constitutes a ferromagnetic sublattice. The total moment cancels out only if Mn1 and Mn2 ordered moments are identical and antiparallel (opposite FM sublattices). In the second model in Table III ($P4'_2m'c$), the moments (as in model_1) only have c-axis component (m_z) . Moreover, each magnetic sublattice (Mn1 and Mn2, separately) adopts an AFM spin configuration. So that the total magnetization in each sublattice and in the whole cell is zero, even if Mn1 and Mn2 sites have slightly different atomic magnetic moments due to their different local environment. Namely, model_2 is not compatible with ferromagnetism. In contrast with the third and fourth polar models ($Cc'c2'$ and $Pm'm2'$), which are both compatible with net ferromagnetism, and where the spins order within the ab plane. Among them, spins in model_3 ($Cc'c2'$) can present components parallel to a and b axes, whereas in model_4 ($Pm'm2'$) the spin ordering is parallel to the crystal a axis (m_x).

Gou *et al.* [10] used first-principles calculations to explore and estimate the magnetic exchange interactions and the relative energy cost associated to different magnetic orderings in $CaMnTi_2O_6$. For that they imposed collinear spin arrangements and considered up to four different configurations of the Mn^{2+} ions in the high-spin state (i.e., both Mn1 and Mn2 sites presenting $S = 5/2$), so-called F, A, C and G. F refers to the full FM configuration, G corresponds to a model in which all first-nearest-neighbors are AFM coupled (in the ab plane and along the columns), so giving an AFM-coupling along the three main axes of the pseudocubic cell. By comparing with the maximal magnetic subgroups described in Table III, one can easily check that the F, A, C and G coupling models considered in Ref. [10], regardless of the easy-axis direction, are particular cases representative of the magnetic symmetries corresponding to, respectively, model_1b, model_2a, model_2b and model_1a in Table III. Based on the structural information, first-principles calculations predicted the energy trend: $E(C) < E(G) < E(F) < E(A)$. Therefore, if one wants to be consistent with these calculations, the magnetic ground state would correspond to the AFM configuration of magnetic space group $P4'_2m'c$ (No. 105.213), the model_2b in Table III. This magnetic order is composed of FM columns of Mn atoms running parallel to the c axis, each column being surrounded by four identical columns with inverted Mn spins relative to the central one. This is the expected magnetic order if, as estimated in Ref. [10], the first dominant magnetic interaction is an in-plane antiferromagnetic exchange between manganese atoms in neighboring Mn columns (AFM interchain coupling), and the second dominant interaction is a ferromagnetic intracolumn exchange (FM intrachain coupling). However, in addition, as shown in Table III, the symmetry of the system forces the C model to align the Mn moments parallel to the c axis. In the same MSG ($P4'_2m'c$) in model_2a the intrachain coupling is AFM and the interchain one is FM. Likewise, the magnetic symmetry $P4_2m'c'$(models_1a and _1b) comprises the cases where the intrachain and interchain interactions have identical sign. Finally, we call the attention to the fact that a key element

to understand the low magnetic ordering temperature is the absence of direct Mn1-O-Mn2 superexchange paths between successive spins along the chains—columns—parallel to c, or between neighboring columns. Namely, magnetic interactions between Mn spins are weak and of supersuperexchange (SSE) type: the magnetic coupling between Mn1 and Mn2 positions takes place through Mn1-O-O- Mn2 supersuperexchange paths exclusively.

IV. CONCLUDING REMARKS

We have confirmed a divalent, high-spin configuration at both so-called square-planar and octahedrally coordinated Mn sites in the ferroelectric $CaMnTi_2O_6$ by means of XAS, as favored by the large ionicity of Mn^{2+}, i.e., with little influence by the oxygen environment. Coherently to this findings, the orbital magnetic contribution was found negligible above T_N, although a sizeable XMCD signal at 5 K gives evidence of a small orbital magnetic moment contribution in the AFM phase [$m_L/m_S = 0.035(3)$]. This reduced value is consistent with a Neel temperature mainly determined by very weak spin-spin exchange interactions between the Mn atoms. The multiplet formalism used to reproduce the experimental XAS and XMCD data across both Ti and Mn $L_{2,3}$ edges reveals that Mn1 and Mn2 sites spectroscopically contribute in a rather similar way. Both experimental and calculated spectra suggest that the PM response from Mn1 and Mn2 sites is balanced and that this does not suffer a major evolution with temperature. Our theoretical analysis points to the latter sites displaying a nominally tetragonal distortion (rather than actual square planar) with $E_{dx2-y2} > E_{dz2} > E_{dxy}$ such that the so-called "$T_d + D_{4h}$ elong" model yields the best results. In contrast, the crystal field produced by O ligands around tetravalent titanium atoms largely determines Ti $L_{2,3}$ XAS spectra. A tiny XMCD signal was recorded at 5 K and 6 T, with spin and orbital magnetic components [$m_S = 0.018(3)$ and $m_L = -0.013(2)\,\mu_B$] nearly cancelling out to produce a practically null atomic moment (within the estimated errors) at Ti sites. The experimental Ti $L_{2,3}$ XAS and XMCD spectra got fairly reproduced assuming a small charge-transfer from O ligands using the CTM formalism.

A FE to PE phase transition is the common response of CMTO to either a temperature [5] or mechanical pressure increase [6], and in both cases the transition is driven by a second-order deactivation of the polar displacements of the eight Ti^{4+} ions along the c direction within their octahedral oxygen framework. In the polar phase this shift is about 0.12 Å, stabilizing the shortest (longest) Ti-O5 apical bonds in 1.836 Å (2.107 Å), the average Ti-O bond length being 1.964 Å. The short Ti-O5 apical bondlenght is also ≈ 0.1 Å smaller than the basal bondlenghts in the TiO_6 octahedron [5]. In this context, it would be of interest to ascertain whether the little O $\rightarrow$ Ti charge-transfer identified in CTM calculations is also present in the non-FE phase, after the suppression of the Ti atomic shift.

The difficulties to prepare enough amount of CMTO, requiring a solid-state reaction under high pressure and temperature, explain the current absence of neutron data that would serve as a basis for the description of the magnetic order in this multiferroic. We thus applied the general principle of maximal symmetry to identify the most favorable magnetic space groups (MSGs) and spin configurations compatible with the polar $P4_2mc$ crystalline structure assuming a zero propagation vector. According to our spectroscopic results, only Mn1 and Mn2 were considered as magnetic sites below T_N. In these conditions, four maximal MSGs were identified as the most probable to occur: $P4_2m'c'$, $P4_2'm'c$, $Cc'c2'$ and $Pm'm2'$. Three of these possible maximal symmetries with null propagation vector present a magnetic point group compatible with a homogeneous magnetization and ferromagnetism. Only in $P4_2'm'c$ null magnetization is symmetry dictated. This MSG corresponds to the C-type spin configuration, predicted to be of lower energy than the G, F, or A collinear magnetic models following first-principles calculations [10], so that the $P4_2'm'c$ symmetry would describe the magnetic ground state. In that case, the symmetry restricts the ordered Mn moments (in both Mn1 and Mn2 sites) along the z axis (only m_z magnetic component). In addition, regarding the columns of Mn atoms along c, the $P4_2'm'c$ symmetry imposes that the coupling between neighboring spins along the columns has the sign reversed respect to the coupling between neighboring chains. To be consistent with the predictions by Gou *et al.* in Ref. [10], the interchain coupling should be antiferromagnetic and the intrachain one ferromagnetic. Namely, tetrahedral Mn1 would be AFM coupled to its four neighbor Mn2 atoms in the ab plane, but the interaction between successive pseudosquare planar Mn2 and tetrahedral Mn1 atoms along c would be FM.

Two-dimensional AFM short-range correlations above T_N are possible according to the magnetic entropy calculations reported by Aimi *et al.* [5]. Given the weak nature of the magnetic coupling in this system (Mn1 and Mn2 positions only interact through super-superexchange paths), there is a high probability of field-induced metamagnetic transitions at moderate external magnetic fields. The XMCD signal observed at 5 K in the Mn $L_{2,3}$ edge indicates a generous magnetic susceptibility from Mn sites. In contrast with the linear field-dependence in the dichroic magnetization loop measured above T_N, the M(H) evolution observed below T_N is nonlinear in the [−2 T, 2 T] range. This observation may suggest a reversible field-induced canting of Mn spins under external field (<2 T), or a spin flip (from $-m_z$ to $+m_z$) of some $S = 5/2$ Mn spins constituting the FM columns parallel to c. At this point, we recall that earlier calculations estimated the intrachain FM exchange fields to be much weaker than the interchain AFM coupling [10]. It is worth noting that the development of a weak FM component has been recently reported in the polymorph $MnTiO_3$-II multiferroic perovskite, which (like CMTO) is based on divalent Mn and tetravalent Ti ions [37]. The weak FM component is perpendicular to the electrical polarization and permits coupled switches of the two ferroic orders. On the other hand, the strikingly low entropy value found in the PM phase of CMTO would support the presence of short-range magnetic order that could see its correlation length enhanced under particular external conditions. Further efforts to overcome the limitations currently found in the production of CMTO may open the door to explore chemical substitutions or mechanical strain with the aim of modifying the optical gap or enhancing the FM correlations, as recently seen in other promising titanates [38].

ACKNOWLEDGMENTS

We thank financial support from the Spanish Ministry of Economy and Competitiveness (MINECO), through projects MAT2015-68760-C2-2-P, MAT2016-75586-C4-1-P/2-P and "Severo Ochoa" Programme for Centres of Excellence in R&D (SEV- 2015-0496). The former is co-funded by ERDF of the European Union. We also acknowledge the ALBA Synchrotron for granting beamtime. J.L.G-M thanks J. M. Pérez-Mato for fruitful discussions and J. H.-M. acknowledges F. M. F. De Groot and S. Agrestini for valuable comments.

[1] J. M. D. Coey, M. Viret, and S. Molnar, Adv. Phys. **48**, 167 (1999).
[2] E. Dagotto, T. Hotta, and A. Moreo, Phys. Rep. **344**, 1 (2001).
[3] S. W. Cheong and M. Mostovoy, Nat. Mater. **6**, 13 (2007).
[4] H. J. Snaith and J. Henry, J. Phys. Chem. Lett. **4**, 3623 (2013).
[5] A. Aimi, D. Mori, K.-i. Hiraki, T. Takahashi, Y. J. Shan, Y. Shirako, J. Zhou, and Y. Inaguma, Chem. Mater. **26**, 2601 (2014).
[6] J. Ruiz-Fuertes, T. Bernert, D. Zimmer, N. Schrodt, M. Koch-Müller, B. Winkler, L. Bayarjargal, C. Popescu, S. MacLeod, and K. Glazyrin, Phys. Rev. B **96**, 094101 (2017).
[7] N. A. Benedek and C. J. Fennie, Phys. Rev. Lett. **106**, 107204 (2011).
[8] N. A. Benedek, A. T. Mulder, and C. J. Fennie, J. Solid State Chem. **195**, 11 (2012).
[9] N. A. Benedek, J. M. Rondinelli, H. Djani, P. Ghosez, and P. Lightfoot, Dalton Trans. **44**, 10543 (2015).
[10] G. Gou, N. Charles, J. Shi, and J. M. Rondinelli, Inorg. Chem. **56**, 11854 (2017).
[11] A. M. Glazer, Acta Crystallogr. B **28**, 3384 (1972).
[12] H. Chen and A. Millis, Sci. Rep. **7**, 6142 (2017).
[13] *Accurate Characterization of the High Pressure Environment*, edited by E. C. Lloyd, Vol. 326 (NBS Special Publication, Washington D.C., 1971).
[14] G. J. Piermarini and S. Block, Rev. Sci. Instrum. **46**, 973 (1975).
[15] J. Susaki, M. Akaogi, S. Akimoto, and O. Shimoura, J. Geophys. Res. Lett. **12**, 729 (1985).
[16] M. Akaogi, H. Yusa, S. Shiraishi, and T. Suzuki, J. Geophys. Res. **100**, 22337 (1995).
[17] A. Barla, J. Nicolás, D. Cocco, S. M. Valvidares, J. Herrero-Martín, P. Gargiani, J. Moldes, C. Ruget, E. Pellegrin, and S. Ferrer, J. Synchr. Rad. **23**, 1507 (2016).
[18] E. Stavitski and F. M. F. De Groot, Micron **41**, 687 (2010).
[19] J. M. I. Aroyo, J. M. Perez-Mato, C. Capillas, E. Kroumova, S. Ivantchev, G. Madariaga, A. Kirov, and H. Wondratschek, Z. Kristallogr. **221**, 15 (2006); also Bilbao Crystallogr. Serv. 2017. MAXMAGN: maximal magnetic space groups for a given a propagation vector and resulting magnetic structural models. *Bilbao Crystallographic Server*. http://www.cryst.ehu.es/cryst/maxmagn.
[20] M. I. Aroyo, A. Kirov, C. Capillas, J. M. Perez-Mato, and H. Wondratschek, Acta Cryst. A **62**, 115 (2006).
[21] J. M. Perez-Mato, S. V. Gallego, E. S. Tasci, L. Elcoro, G. de la Flor, and M. I. Aroyo, Annu. Rev. Mater. Res. **45**, 217 (2015).
[22] ISOTROPY Software Suite, iso.byu.edu. B. J. Campbell, H. T. Stokes, D. E. Tanner, and D. M. Hatch, J. Appl. Cryst. **39**, 607 (2006).
[23] Rigaku, CRYSALIS*Pro* software system, version 1.171.36.28, Rigaku Technologies UK Ltd. (2013).
[24] G. M. Sheldrick, Acta Crystallogr., Sect. A **64**, 112 (2008).
[25] F. De Groot and A. Kotani, *Core Level Spectroscopy of Solids* (Taylor and Francis, New York, 2008).
[26] S. P. Cramer, F. M. F. de Groot, Y. Ma, C. T. Chen, F. Sette, C. A. Kipke, D. M. Eichhorn, M. K. Chan, W. H. Armstrong, E. Libby, G. Christou, S. Brooker, V. McKee, O. C. Mullins, and J. C. Fuggle, J. Am. Chem. Soc. **113**, 7937 (1991).
[27] B. T. Thole, P. Carra, F. Sette, and G. van der Laan, Phys. Rev. Lett. **68**, 1943 (1992).
[28] C. T. Chen, Y. U. Idzerda, H.-J. Lin, N. V. Smith, G. Meigs, E. Chaban, G. H. Ho, E. Pellegrin, and F. Sette, Phys. Rev. Lett. **75**, 152 (1995).
[29] Parameters employed (eV) for Mn1: T_d symmetry, $10Dq = -0.5$, Ds = Dt = 0; for Mn2: C_{4h} symm., $10Dq = 0.5$, Ds = 0.05, Dt = 0; for Ti: C_{4h} symm., $10Dq = 2.2$, Ds = 0.1, Dt = 0.06, Δ; $(C - T) = 3.0$, $U_{cd} - U_{dd} = 2.0$. In all cases, $M = 1$ meV.
[30] G. Van der Laan and I. W. Kirkman, J. Phys: Cond. Matter **4**, 4189 (1992).
[31] T. Fujii, M. Yamashita, S. Fujimori, Y. Saitoh, T. Nakamura, K. Kobayashi, and J. Takada, J. Magn. Magn. Mater. **310**, e555 (2007).
[32] H. Ikeno, T. Matoba, T. Mizoguchi, I. Tanaka, T. Nakamura, Y. Takeda, T. Okane, and K. Tanaka, Appl. Phys. Lett. **104**, 112408 (2014).
[33] F. M. F. de Groot, J. C. Fuggle, B. T. Thole, and G. A. Sawatzky, Phys. Rev. B **41**, 928 (1990).
[34] D. Pesquera, M. Scigaj, P. Gargiani, A. Barla, J. Herrero-Martín, E. Pellegrin, S. M. Valvidares, J. Gázquez, M. Varela, N. Dix, J. Fontcuberta, F. Sánchez, and G. Herranz, Phys. Rev. Lett. **113**, 156802 (2014).
[35] H. Ikeno, J. Appl. Phys. **120**, 142104 (2016).
[36] N. V. Belov, N. N. Neronova, and T. S. Smirnova, Sov. Phys. Crystallogr. **2**, 311 (1957).
[37] A. M. Arévalo-López and J. P. Attfield, Phys. Rev. B **88**, 104416 (2013)..
[38] E. Gradauskaite, J. Gardner, R. M. Smith, F. D. Morrison, S. L. Lee, R. S. Katiyar, and J. F. Scott, Phys. Rev. B **96**, 104104 (2017).